

## Thermal accommodation of spin-polarized hydrogen on liquid-He surfaces below 0.25 K

J. A. Helffrich\* and M. P. Maley

*Physics Division, Los Alamos National Laboratory, Los Alamos, New Mexico 87545*

M. Krusius

*Los Alamos National Laboratory, Los Alamos, New Mexico 87545*

*and Low Temperature Laboratory, Helsinki University of Technology, SF-02150 Espoo, Finland*

(Received 26 January 1990)

We have measured the thermal accommodation of spin-polarized hydrogen gas on superfluid He films at saturation thickness in the temperature range 0.1–0.25 K. The measurements have been performed as a function of  $^3\text{He}$  concentration by monitoring the thermal flux between two parallel plates maintained at slightly differing temperatures. The measuring arrangement was designed to secure homogeneous  $^3\text{He}$  coverages and to minimize uncontrolled thermal gradients. No dependence of the accommodation coefficient on the  $^3\text{He}$  concentration is observed within the resolution of the measurements of  $\pm 30\%$ . The results are consistent with recent surface-sticking measurements, assuming that thermal accommodation proceeds on both  $^3\text{He}$  and  $^4\text{He}$  surfaces via sticking-evaporation collisions; i.e., inelastic surface scattering is negligible.

### I. INTRODUCTION

In a recent experiment<sup>1</sup> we measured the thermalization of atomic hydrogen on the surface of a saturated superfluid  $^4\text{He}$  film, expressed in terms of the energy accommodation coefficient  $\alpha(T)$ , and found it to decrease rapidly with decreasing temperature, varying as  $\alpha = 0.50T$  over the temperature range  $0.18 < T < 0.40$  K. This result is in good agreement with Statt's<sup>2</sup> calculated  $\alpha(T)$ , which in turn is based on an earlier calculation of H atom sticking by Zimmerman and Berlinsky.<sup>3</sup> The sticking coefficient  $s(T)$  has recently also been measured by Berkhout *et al.* by monitoring the H atom flow through a superfluid- $^4\text{He}$ -film-coated glass capillary tube, and the result  $s = 0.33T$  was obtained for the temperature interval  $0.145 < T < 0.526$  K.<sup>4</sup> Provided that H atom thermalization on the liquid- $^4\text{He}$  surface is dominated by sticking-evaporation collisions, then these recent measurements of  $\alpha(T)$  and  $s(T)$  are in perfect agreement, since, for linear temperature dependencies, the two quantities are related as  $\alpha = 3s/2$ .<sup>5</sup> The H gas-liquid  $^4\text{He}$  surface interaction via the sticking-evaporation channel is mediated by the emission and absorption of a single ripplon. This process has been shown to be much more efficient than inelastic nonsticking collisions by the same energy exchange mechanism.<sup>6</sup> According to Statt's estimate,<sup>2</sup> the inelastic contribution to thermalization only amounts to  $\alpha_{\text{in}} = 0.011T^2$ . It would thus appear that the H gas-liquid  $^4\text{He}$  surface interactions are well understood.

H atom thermalization on the liquid- $^3\text{He}$  surface is not so well understood. It is well known that propagating low-frequency capillary waves can be excited and observed on the free surface of bulk liquid  $^3\text{He}$ , whereas high-frequency ripplon excitations are predicted to be heavily damped due to the large viscosity of the normal  $^3\text{He}$ .<sup>7,8</sup> At first sight one might suspect that inelastic sur-

face collisions involving quasiparticle excitations could in this situation become effective in the thermalization process. On the other hand, it is conceivable that the long thermal wavelength of the H atom precludes hard core collisions with the  $^3\text{He}$  surface atoms and that quasiparticle creation remains a relatively inefficient mechanism. One would then expect to find a reduced accommodation coefficient on the bulk liquid- $^3\text{He}$  surface as compared to  $^4\text{He}$ , primarily because of the reduction in the adsorption energy by a factor of 3. The absence of detailed calculations for the  $^3\text{He}$  surface and limited experimental information lead to a high degree of uncertainty concerning the relative magnitudes of thermal accommodation and sticking on the two He surfaces. This, of course, would be valuable knowledge in selecting the most promising environment and experimental procedure for approaching the Bose-Einstein condensation limit in the spin-polarized  $\text{H}_1$  gas. The advantage in using a  $^3\text{He}$  surface is the lower H atom adsorption energy and a reduced surface recombination rate, which dominates losses and heating in  $\text{H}_1$  gas at the lowest temperatures.

The experimental information on thermal accommodation and sticking on  $^3\text{He}$  containing surfaces is inadequate and, in particular, does not include the free surface of bulk liquid  $^3\text{He}$ . Jochemsen *et al.*<sup>9</sup> have performed NMR measurements on dissociated H atoms in a sealed glass bulk, initially filled at room temperature with a small charge of  $\text{H}_2$  and  $^4\text{He}$  or  $^3\text{He}$  gas. An analysis of NMR linewidths gave  $s = 0.046$  in the presence of  $^4\text{He}$  at 0.2 K, while, with  $^3\text{He}$  at 0.1 K,  $s = 0.016(5)$  was obtained. Both of these results are from the temperature region in which later measurements give a sticking coefficient  $s \propto T$ , and, thus, they could be interpreted to yield a somewhat lower value for  $^3\text{He}$  than for  $^4\text{He}$ . However, in this experiment the  $^3\text{He}$  coating is an immobile film, only a few monolayers thick, while the standard  $\text{H}_1$  setup employs a saturated superfluid-He-film lining to

reduce recombination losses. The capillary-flow measurements of Berkhout *et al.*<sup>4</sup> were conducted on such a substrate and their results show that  $s(T)$  is independent of  $^3\text{He}$  concentration in the temperature range  $0.073 < T < 0.174$  K. In order to examine these inconsistencies we have determined  $\alpha(T)$  at several  $^3\text{He}$  concentrations using a different measuring arrangement that secures well-controlled stationary-state conditions for the accommodation measurements below 0.25 K. We employ a parallel-plate geometry in order to minimize thermal gradients and to improve the homogeneity of the  $^3\text{He}$  coverage. Furthermore, the lower plate forms the bottom cover of the  $\text{H}_1$  cell, and thus this arrangement allows the use of thick  $^3\text{He}$  layers on one of the active surfaces. The upper plate, similar to all other surfaces in the cell above the pool of liquid on the bottom plate, carries a superfluid  $^4\text{He}$  film at saturation thickness with varying amounts of  $^3\text{He}$  particles residing in a two-dimensional gaseous state on the surface. The density of the  $^3\text{He}$  layer increases exponentially with decreasing temperature and, eventually at about 0.1 K, will reach that of a full monolayer. Nevertheless, we find that our results are very similar to those of Berkhout *et al.*;<sup>4</sup> namely that, on adding  $^3\text{He}$  into the  $\text{H}_1$  cell, little if any change is observed in  $\alpha(T)$  from the behavior measured for a pure  $^4\text{He}$  film.

A number of different measurements on the surface properties of bulk liquid- $^3\text{He}$ - $^4\text{He}$  mixtures and their films at saturation thickness have demonstrated that the appearance of a dense  $^3\text{He}$  coverage is prominently manifested in both the static and dynamic properties below 0.3 K.<sup>7</sup> For example, the surface tension decreases monotonically from the pure  $^4\text{He}$  value with increasing  $^3\text{He}$  coverage and the increasing diffusiveness of the surface profile. A thermal current on the saturated superfluid  $^4\text{He}$  film is transmitted by a flux of ripples, which, however, is rapidly attenuated in the presence of a  $^3\text{He}$  surface layer by  $^3\text{He}$  quasiparticle excitations. This gaseous two-dimensional Fermi system supports surface second sound modes, which are propagating longitudinal compressional waves in the  $^3\text{He}$  density that, in contrast to ripples, do not involve vertical displacements. They can be excited and detected thermally.<sup>10</sup> This description in terms of submonolayer coverages of  $^3\text{He}$  should apply to all of our  $^3\text{He}$  concentrations except for the  $> 6.4\%$  solution, which is expected to present a bulk  $^3\text{He}$  surface. In view of these observations, which all underline the large difference in the properties of the pure  $^4\text{He}$  surface and the  $^3\text{He}$  covered surface, it appears surprising that surface interactions with H atoms should be so similar. In particular, since these interactions on the  $^4\text{He}$  surface are dominated by sticking-evaporation collisions, according to the results of the sticking and the accommodation measurements, the most important single parameter should be the adsorption energy  $\epsilon_a$ . It has been measured to have rather different values for the  $^4\text{He}$  surface ( $\cong 1.0$  K) and the saturated  $^3\text{He}$ - $^4\text{He}$  film ( $\cong 0.34$  K);<sup>11</sup> which becomes distinctly apparent in any experiment with  $\text{H}_1$  from the greatly reduced surface recombination rate in the presence of a mixture film.

The present results show that the accommodation coefficient is  $^3\text{He}$ -concentration independent to within

$\pm 30\%$ . Several factors contribute to the wide uncertainty range. First, the data for the pure  $^4\text{He}$  and the  $^3\text{He}$  covered surfaces overlap poorly. The measurement on the  $^4\text{He}$  surface runs into difficulties below 0.2 K where H adsorption and subsequent recombination in the densely populated adsorbed  $\text{H}_1$  phase produces large heat flows. On the other hand, the measurements on the  $^3\text{He}$ - $^4\text{He}$  mixture films have to be conducted below 0.2 K in order to avoid problems associated with the higher vapor pressure of  $^3\text{He}$  and also to secure a dense enough  $^3\text{He}$  coverage on the film. Thus, the fact that this comparison has to be performed in just the same temperature interval where the  $^3\text{He}$  surface layer starts to approach monolayer density creates obvious difficulties. For instance, all of the recent measurements have used only nominally pure  $^4\text{He}$ , in which the contamination from the natural abundance of the  $^3\text{He}$  isotope is sufficient to produce sizable coverages below 0.2 K. Therefore, the "pure"  $^4\text{He}$  surface will ultimately resemble that of the  $^3\text{He}$  containing films. Furthermore, the extrapolation of the existing measurements to lower temperatures for a  $^4\text{He}$  surface may not necessarily be a straightforward continuation of the measured linear  $\alpha = 0.50T$  dependence, with an expected turnover to the  $\alpha \propto \sqrt{T}$  dependence at the very lowest temperatures.<sup>3</sup> Below 0.2 K the ripplon mediated sticking collision becomes sensitive to the long-range part of the H-atom-He-surface potential; depending on the choice of ansatz for the surface potential, widely varying temperature dependencies for the calculated  $\alpha(T)$  and  $s(T)$  are obtained, as has been demonstrated by both Statt<sup>2</sup> and Goldman.<sup>5</sup>

Nevertheless, in spite of these complications which contribute to the wide uncertainty limits, the weak dependence of the H atom thermalization properties on the composition of the liquid-He adsorbate surface is unexpected. We shall return to this question in Sec. VI. In Secs. II-IV, we discuss the technique and the technical details of our accommodation measurements, and in Sec. V, the experimental data are presented.

## II. PRINCIPLE OF THE MEASUREMENT

The thermal accommodation measurement is performed under steady-state conditions at low gas density, where the mean free path is longer than the cell dimensions. We can then write for the heat flux conducted from a hot point source at the temperature  $T_s$  to the cold walls at  $T_c$ :

$$Q_H = \frac{1}{4}n(T_c)\bar{v}(T_c)\alpha 2k_B(T_s - T_c)A_s. \quad (1)$$

Here

$$\bar{v}(T_c) = (8k_B T_c / \pi m_H)^{1/2}$$

is the mean atomic speed, and  $\Phi_H = \frac{1}{4}n\bar{v}$  is the H atom flux per unit area hitting the hot surface, while  $2k_B T_c$  is the average kinetic energy delivered by this flux with a Maxwellian velocity distribution centered at the cell temperature  $T_c$ . Thus, the thermal accommodation coefficient  $\alpha$  is defined as the ratio of the actual heat flux  $Q_H$  to the maximum possible flux  $\Phi_H 2k_B(T_s - T_c)A_s$ . It

is assumed that all incident atoms have been thermalized to the cell temperature, which means that the surface area  $A_s$  of the hot point-source-like sensor has to be much smaller than that of the surrounding cell.

In order to secure an equilibrium  $^3\text{He}$  film coverage, we chose to employ a parallel-plate configuration instead. Nevertheless, Eq. (1) is still valid if we replace  $\alpha$  with an effective accommodation coefficient  $\alpha_{\text{eff}}$  and express the particle flux

$$\Phi_H = \frac{1}{4}n(T)\bar{v}(T)$$

at an average gas temperature  $T_m$ .

Kennard<sup>12</sup> has shown, for the parallel-plate geometry, that

$$\alpha_{\text{eff}} = \frac{\alpha_c \alpha_s}{\alpha_c + \alpha_s - \alpha_c \alpha_s} . \quad (2)$$

In the present situation the hot and cold surfaces are generally identical, except for their temperatures, and moreover, given the linear temperature dependence of  $\alpha(T)$  according to Ref. 1, we may write  $\alpha = \alpha_0 T$  (with  $\alpha_0 = \text{constant}$ ) within a narrow temperature span  $T_c < T < T_s$ . With good accuracy it then follows that

$$\alpha_{\text{eff}} = \frac{\alpha}{2 - \alpha} , \quad (3)$$

where  $\alpha = \alpha_0 T_m$  and  $T_m$  is the arithmetic mean  $T_m = (T_c + T_s)/2$ . Thus by measuring the amount of heat  $Q_H$ , which is carried from the hot sensor plate per unit time via H atom conduction,

$$Q_H = \frac{1}{2} \alpha_{\text{eff}} n(T_c) \bar{v}(T_c) k_B (T_s - T_c) A_s , \quad (4)$$

we obtain  $\alpha_{\text{eff}}$  and from Eq. (3) the corresponding accommodation coefficient  $\alpha$ , which is assigned the temperature  $T_m$ . In Eq. (4) we have used the fact that, in a gaseous system in the ballistic flight regime, and in the presence of an inhomogeneous temperature distribution, the conserved quantity is the flux; and therefore

$$n(T_H) \bar{v}(T_H) = n(T_c) \bar{v}(T_c) .$$

From a practical point of view Eq. (4) is now expressed in suitable form, directly amenable to measurement:  $Q_H$  is the additional electrical heating that has to be supplied to the sensor plate in order to maintain its temperature at  $T_s$  when the H gas charge is admitted into the  $\text{H}_1$  cell; the cell temperature  $T_c$  is measured with a  $^3\text{He}$  melting pressure gauge, the sensor temperature  $T_s$  with a resistance thermometer glued to the sensor plate, and the gas density  $n(T_c)$  with a manometer.

Only in the case when the hot sensor plate on the bottom of the cell is covered with a phase-separated layer of concentrated  $^3\text{He}$  liquid are the two surfaces of dissimilar nature. We then obtain from Eq. (2) the unknown  $\alpha_s$  for the bulk  $^3\text{He}$  surface by inserting the measured  $\alpha_{\text{eff}}$  and the appropriate value for  $\alpha_c$ , given by measurements with a small amount of  $^3\text{He}$  in the cell.

### III. DETAILS OF THE MEASUREMENT PROCEDURE

An important consideration in the parallel-plate arrangement is the need to minimize lateral heat flow while each of the two plates is still kept isothermal. As shown in Fig. 1, this requirement is accomplished by dividing the lower, heated plate into a central sensor area and a surrounding concentric annular guard ring. Both sensor and guard have been prepared from 25- $\mu\text{m}$ -thick copper foil, epoxy laminated onto a 25- $\mu\text{m}$  Kapton foil support, which also forms the vacuum-tight bottom cover of the  $\text{H}_1$  cell. Separate resistive heater and thermometer elements have been glued to the back sides of the sensor and the guard where they face a vacuum space. Prior to introducing  $\text{H}_1$  the sensor plate can be maintained at  $T_s$  entirely by the guard heater, but, in the presence of a  $\text{H}_1$  sample, additional heating  $Q_{\text{ex}}$  has to be supplied to the sensor heater in order to compensate for the gas conduction:

$$Q_{\text{ex}} = Q_H(T_s) - Q_{\text{rec}}(T_s), \quad \text{with } \text{H}_1 \text{ and } T_g = T_s . \quad (5)$$

Here  $Q_{\text{rec}}$  is an unknown amount of recombination heating.  $Q_{\text{ex}}$  is recorded as a function of time while the  $\text{H}_1$  sample is decaying, typically by a factor of 4 in density around  $n \approx 1 \times 10^{14} \text{ H/cm}^3$ . The measurement is next repeated with a new  $\text{H}_1$  sample decaying over the same density range, but in the absence of any external heating applied to either the guard or the sensor. In this case the energy balance for the sensor reads

$$Q_H(T'_s) + Q_{\text{lat}}(T'_s, T'_g) = Q_{\text{rec}}(T'_s), \quad \text{with } \text{H}_1 \text{ and } Q_{\text{ex}} = 0 , \quad (6)$$

where  $T'_s$  and  $T'_g$  are the measured sensor and guard temperatures, raised by the recombination heating slightly above  $T_c$ . The lateral heat flow from the sensor  $Q_{\text{lat}}(T'_s, T'_g)$  is measured by monitoring the heating  $Q'_{\text{ex}}$  required to maintain the sensor at  $T'_s$  in the empty cell

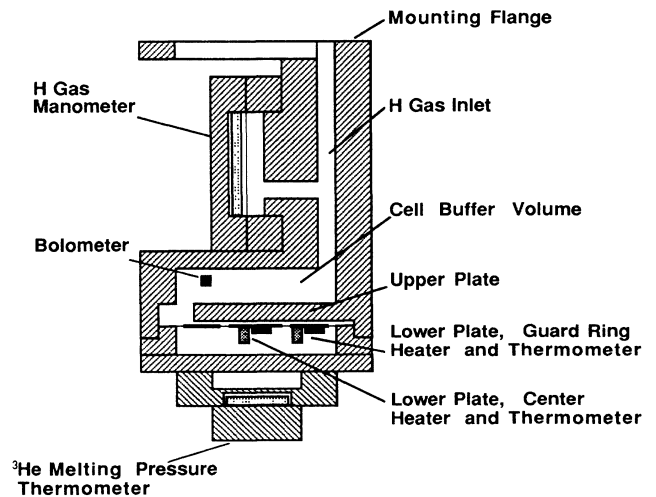


FIG. 1.  $\text{H}_1$  sample chamber for thermal accommodation measurements with parallel-plate configuration.

with the guard heated to  $T'_g$ :

$$Q'_{\text{ex}} = Q_{\text{lat}}(T'_s, T'_g), \text{ no } H_{\downarrow} \text{ and } T_g = T'_g. \quad (7)$$

For simplicity we equate

$$Q_{\text{rec}}(T_s) = Q_{\text{rec}}(T'_s)$$

and Eqs. (4)–(7) can now be solved self-consistently for  $\alpha_{\text{eff}}$ .

In this analysis we have neglected a small dependence of the recombination heating on the sensor temperature, as suggested by the following considerations: (i) The recombination energy can be considered to be uniformly distributed on all surfaces inside the cell, even in the presence of minor inhomogeneities in surface temperature, since only a negligible fraction of the recombination energy is released at the initial surface recombination site. (ii) The total recombination rate in the cell undergoes only a minor change when the guard and the sensor are heated to  $T_s$  as the temperature difference  $T_s - T_c \simeq 10\text{--}40$  mK is small and the combined area of the sensor and the guard is only 6% of the free surface in the cell. (iii) Finally, our approach is to allow the sample to decay towards a doubly polarized, low-density state where the heating from the residual surface recombination, proportional to  $n^2$ , becomes unimportant compared to  $Q_H(T_s)$ . Thus the decaying  $H_{\downarrow}$  samples are monitored over time spans ranging from hours at high temperatures to several minutes at our lowest cell temperature (0.15 K for a  ${}^4\text{He}$  film and 0.09 K for  ${}^3\text{He}$ - ${}^4\text{He}$  mixture films).

Two further corrections, which were important in our previous thermal accommodation measurement,<sup>1</sup> are here found to be unnecessary. First, at these temperatures, evaporation cooling is negligible. Second, the Kapitza thermal boundary resistance between the sensor and the He film was investigated by filling the cell with  ${}^4\text{He}$  and measuring the thermal resistance from sensor to cell, which was found to be negligible.

Finally, we note that the use of a guard ring eliminates lateral heat flow to first order but a small problem remains, nevertheless. When the cell is filled with a  $H_{\downarrow}$  sample, the 1-mm-wide isolation gap between sensor and guard develops a near parabolic temperature distribution which is controlled by the interplay between cooling from gas conduction and heating from lateral conduction. By solving this one-dimensional thermal diffusion problem, it can be shown that to first order the residual lateral heat flow from the sensor into the isolation gap can be accounted for by substituting for the sensor area  $A'_s = \pi R_s R_g$ , where  $R_s$  and  $R_g$  are the inner and outer radii of the thermal isolation gap (here  $R_s = 6.5$  mm and  $R_g = 7.5$  mm).

#### IV. CELL AND SENSOR CONSTRUCTION

The  $H_{\downarrow}$  system employed in this measurement is cooled with a dilution refrigerator and consists of a superfluid-He-temperature dissociator and the  $H_{\downarrow}$  cell. The latter is both mechanically and thermally connected to the mixing chamber by means of a massive Cu yoke, which supports the cell in the center of a superconducting solenoid. The

magnet is located outside the vacuum jacket in the liquid-He bath and maintains a persistent field of 8.0 T. The design and properties of the  $H_{\downarrow}$  dissociator have been reported in Ref. 13.

The  $H_{\downarrow}$  cell, shown in Fig. 1, is made of thick copper to secure good thermal homogeneity between its three principal components: the thermal accommodation volume, the capacitive  $H_{\downarrow}$  pressure gauge, and the  ${}^3\text{He}$  melting pressure thermometer. Sintered heat exchangers, cold welded by pressing 700 Å silver powder into annular slots in the cell body, provide thermal contact between the superfluid-He-film coating in the  $H_{\downarrow}$  volume and the  ${}^3\text{He}$  liquid-solid mixture in the melting pressure gauge. The pancake-shaped space reserved for the accommodation measurement is bounded by a thick copper partition wall towards the main  $H_{\downarrow}$  volume above it and by the Kapton foil and copper sensor and guard plates forming the vacuum-tight bottom cover of the  $H_{\downarrow}$  system. The separation of these two surfaces is 0.9 mm. Interconnections for gas flow between different parts of the  $H_{\downarrow}$  system inside the cell body are provided by tubular ducts, 3–6 mm in diameter. The use of separate heating and temperature sensing elements on both the sensor and the guard ring allows us to locate these on the lower side of the Kapton foil. The heaters are painted colloidal graphite (Aquadag) films, and the thermometers are miniature  $\text{RuO}_2$  thick-film resistor chips.<sup>14</sup> All have thermal resistances to their respective copper plates above the Kapton foil of roughly  $1 \times 10^5$  K/W, which is comparable to the  $4 \times 10^5$  K/W resistance measured at 0.12 K between sensor and guard ring. At an excitation level of  $10^{-13}$  W to the thermometers, the temperature difference between the chip and the copper plate is negligible, and stable, reproducible temperature readings can still be recorded with  $\pm 0.1$ -mK accuracy.

With decreasing temperature the limiting factor in the accommodation measurement becomes the sensitivity and stability of the  $H_{\downarrow}$  manometer. The moving electrode of our capacitive membrane gauge is an evaporated gold layer on a Kapton foil of 22-mm diameter and 12.5- $\mu\text{m}$  thickness. The capacitance, which at zero pressure difference reads 120 pF and has a pressure dependence of  $(60 \pm 0.1)$  fF/Torr, is read with an ac bridge circuit employing a seven-decade inductive ratio transformer and a transformer coupled drive at 2 kHz and 3.5 V rms.<sup>15</sup> With feedback control the drive voltage is stabilized to 10 ppm, which reduces the drift of the bridge balance to below the overall resolution of  $\Delta C/C \sim 10^{-8}$  (or  $\Delta n \sim 5 \times 10^{11}$  H/cm<sup>3</sup> at 0.2 K). Mechanical stress in the membrane is released with a time constant of roughly one week; it gives rise to a drift in the bridge balance of  $\Delta C/C \sim 10^{-7}$  over 12 h, which can be subtracted from the bridge readings. The manometer is calibrated against the vapor pressure of  ${}^4\text{He}$  in the temperature interval 0.40–0.70 K with a large amount of  ${}^4\text{He}$  in the  $H_{\downarrow}$  system. It can then be used for monitoring both the  $H_{\downarrow}$  density and the thickness of the superfluid  ${}^4\text{He}$  film coating.

The film thickness has to be carefully monitored while  ${}^4\text{He}$  is admitted into the  $H_{\downarrow}$  system, either by vapor pressure measurement or by recording one of the thermal resistances, e.g., between sensor and guard ring. Once

saturation is reached, all additional  $^4\text{He}$  accretes on the bottom of the cell and rapidly shorts out the thermal resistances. A buffer volume of  $0.02\text{ cm}^3$  of  $^4\text{He}$  is provided by the heat exchange sinter, which fills by capillary condensation before saturation conditions are reached. When  $^3\text{He}$  is added to the system it first preferentially binds to the free surface of the  $^4\text{He}$  film, with a binding energy of  $2.2\text{ K}$  relative to the dissolved state.<sup>7</sup> Thus, the free surface of  $80\text{ cm}^2$  will start to load up with  $^3\text{He}$  with exponential temperature dependence and will approach full monolayer coverage with a minimum of 100-ppm concentration below about  $0.1\text{ K}$ . All additional  $^3\text{He}$  will dissolve in  $^4\text{He}$  with a binding energy of  $2.8\text{ K}$  with respect to the vacuum, until the solubility limit of  $6.4\%$  is reached. Beyond this, the added  $^3\text{He}$  must go into the concentrated  $^3\text{He}$  surface layer on the bottom plates of the cell, making this layer macroscopically thick. In the presence of inhomogeneities in the surface temperature, gradients in the  $^3\text{He}$  concentration will build up for submonolayer coverages.<sup>16</sup> This is, in fact, the case in any steady-state accommodation measurement between  $0.1$  and  $0.2\text{ K}$ . In the guarded, parallel-plate arrangement the concentration gradients can be kept at a minimum, since a small temperature difference can be used ( $\Delta T/T \approx 0.1$ ), and the geometry allows efficient flow for establishing the equilibrium concentration distribution. In the present measurements only the initial  $^4\text{He}$  charge, with the natural isotopic abundance of  $^3\text{He}$ , is below the 100-ppm limit by about two orders of magnitude; all other concentrations are well above. However, the evolution of the surface coverage is both density and temperature dependent, and thus the monolayer density is only gradually built up with increasing  $^3\text{He}$  concentration at our measuring temperatures of  $T > 0.1\text{ K}$ . The maximum concentration of  $\geq 6.4\%$  is chosen to be above the solution limit such that a macroscopically thick  $^3\text{He}$  layer exists on the bottom plate.

## V. EXPERIMENTAL RESULTS

As a consistency check between our earlier accommodation measurements with a pointlike heat source<sup>1</sup> and the present parallel-plate experiment, we performed the first runs with nominally pure  $^4\text{He}$ . The results are shown in Fig. 2 together with the data from Ref. 1. The agreement is good; the comparison indicates that both techniques have been perfected to a similar degree. In spite of the more refined instrumentation and a more advantageous measuring geometry, the new results extend only slightly lower in temperature ( $0.15\text{ K}$  versus  $0.18\text{ K}$  in Ref. 1). This is due to the difficulties brought about by the exponentially increasing surface recombination and the loss of gas-phase density towards lower temperatures, which combine to rapidly reduce resolution in the density measurement.

Next, increasing amounts of  $^3\text{He}$  were admitted to the  $\text{H}_1$  system to form solutions varying in concentrations from 200 ppm to  $6.4\%$ , as determined by comparing their vapor pressures with the calculated values of Radebaugh<sup>17</sup> at temperatures between  $0.2$  and  $0.3\text{ K}$ . The measured accommodation coefficients for these mixtures

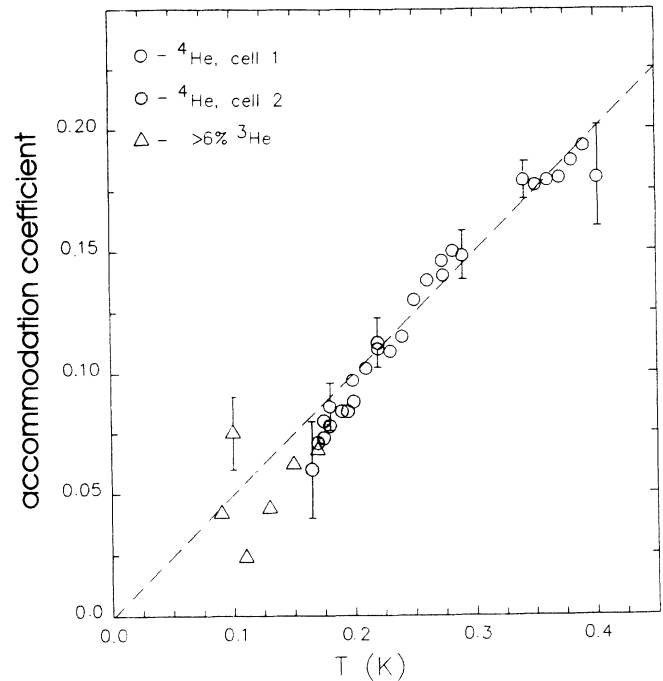


FIG. 2. Thermal accommodation coefficient  $\alpha(T)$  vs temperature for a nominally pure  $^4\text{He}$  surface: open circles, data from Ref. 1; solid circles, present measurements; dashed line,  $\alpha=0.50T$ . Additionally for comparison: triangles, concentrated  $^3\text{He}$  phase on a  $>6.4\%$   $^3\text{He}$ - $^4\text{He}$  mixture. The error bars denote the estimated experimental uncertainty limits.

at two mean temperatures of  $0.15$  and  $0.17\text{ K}$  are shown in Fig. 3 as a function of concentration. Our commercial  $^4\text{He}$  is expected to contain less than  $1\text{ ppm}$  of  $^3\text{He}$ . To obtain an estimate of the bulk concentration needed for reaching the monolayer completion on the surface at these temperatures, we use the data measured for the reduction in the surface tension as a function of temperature at different  $^3\text{He}$  concentrations by Guo *et al.*<sup>18</sup> At the three surface temperatures of  $0.14$ ,  $0.16$ , and  $0.18\text{ K}$ , which have been used in the measurements of Fig. 3, monolayer coverage is obtained with  $0.07\%$ ,  $0.08\%$ , and

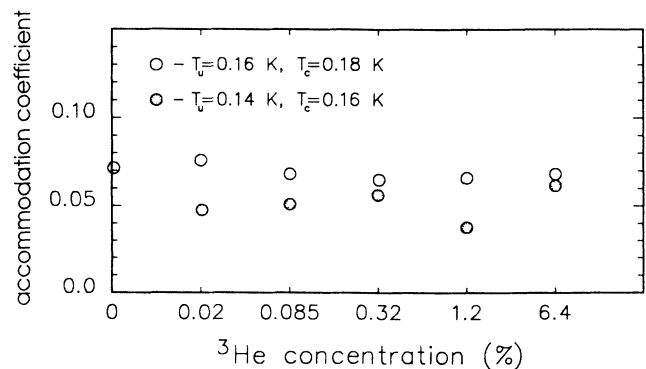


FIG. 3. Thermal accommodation coefficient vs  $^3\text{He}$  concentration at two different mean temperatures: solid circles,  $0.15\text{ K}$ ; open circles,  $0.17\text{ K}$ .

0.10% of  $^3\text{He}$ , respectively. Thus, the formation of a dense  $^3\text{He}$  coverage falls in the low-concentration region of Fig. 3, while the saturated solution of 6.4% corresponds already to the situation where a phase-separated layer of concentrated  $^3\text{He}$  liquid resides on the bottom plate. There is no doubt about the presence of the  $^3\text{He}$  coverage in these measurements; it is plainly evident in the much-reduced recombination rate and the higher gas-phase density under otherwise corresponding conditions. On comparing with the indicated estimates of the uncertainty limits for the data in Fig. 3 we may conclude that the  $^3\text{He}$  coverage dependence of  $\alpha$  is less than the resolution in the measurement, estimated as  $|\Delta\alpha/\alpha| \cong \pm 30\%$ .

Finally, in Fig. 4 all of the mixture data along with results for the pure  $^4\text{He}$  surface from Ref. 1 are shown as a function of temperature to illustrate the fact that the concentration dependence is smaller than the scatter of the data. The results fall below the linear dependence  $\alpha=0.50T$ , which was obtained in the measurements of Refs. 1 and 4. Comparing Figs. 2 and 4, we note that the departure from the dashed line below 0.2 K is present to a similar degree in the data measured for the nominally pure  $^4\text{He}$  surface as well as the  $^3\text{He}$ - $^4\text{He}$  mixtures. At present, it is not clear whether this trend at the lowest temperatures is significant or not; it was not observed in the capillary-flow measurements of the sticking coefficient in Ref. 4. Estimates of the experimental uncertainties are indicated with error bars in Fig. 2. At the lowest

temperatures and the highest  $^3\text{He}$  concentration the scatter is outside of these; we feel that this is due to thermal effects from temporal variations in  $^3\text{He}$  concentration, which have frequently been seen under similar conditions at saturated film thickness<sup>19</sup> and which constitute powerful sources of heat.

## VI. DISCUSSION

We have measured the thermal accommodation of hydrogen atoms on a  $^3\text{He}$  surface and compared the results with those of a similar investigation on  $^4\text{He}$  surfaces. The experiment was designed to ensure a  $^3\text{He}$  coverage on the sensor surface in the presence of small thermal gradients. Recombination decay rates in the temperature range 0.1–0.2 K were consistent with those previously observed on  $^3\text{He}$ -covered surfaces and with an adsorption energy for the hydrogen  $\sim 0.35$  K. For concentrations  $< 6.4\%$ , we were measuring thermal accommodation on a two-dimensional gas of  $^3\text{He}$  adsorbed onto the underlying  $^4\text{He}$  surface; and for the  $> 6.4\%$   $^3\text{He}$  solutions, we should have obtained a bulk  $^3\text{He}$  surface. We find that our results are independent of  $^3\text{He}$  concentration to within the experimental errors.

In temperature dependence, our measurements lie somewhat below the  $\alpha(T)=0.5T$  dependence previously established for  $^4\text{He}$  surfaces in the temperature range of 0.18–0.4 K. The observation of monotonically decreasing sticking and thermal accommodation with decreasing temperature agrees with the predictions of the one-rippion sticking and evaporation model. More generally, the increasing surface reflection is the result of the increasing mismatch between the long wavelengths of the incoming atoms and the short wavelengths they have when adsorbed. However, even at the lowest temperatures measured, we have not obtained the limiting  $\sqrt{T}$  dependence that is a general feature of these models.

As demonstrated by Goldman,<sup>5</sup> the low-temperature dependence of sticking and accommodation in the one-rippion model is very sensitive both to the repulsive core strength, i.e., the penetration energy of the H atom into the bulk liquid, and to the long-range behavior of the surface interaction. The limited temperature range of our measurements does not allow any general conclusions to be made concerning the form of this potential appropriate to the  $^3\text{He}$  or  $^4\text{He}$  surfaces.

As previously discussed, the different physical properties of the  $^3\text{He}$  and  $^4\text{He}$  surfaces, e.g., density, hydrogen atom binding energy, surface tension, and viscosity, suggest the possibility of different sticking and accommodation mechanisms. In particular, mechanisms involving transfer of energy to single-particle excitations and surface acoustic waves are possibilities. In the absence of detailed calculations, it is difficult to assess the probability that these will be efficient means of producing sticking and accommodation. It seems improbable that such fundamentally different mechanisms would produce the similar values for  $\alpha(T)$  for  $^3\text{He}$  and  $^4\text{He}$  over the temperature ranges investigated.

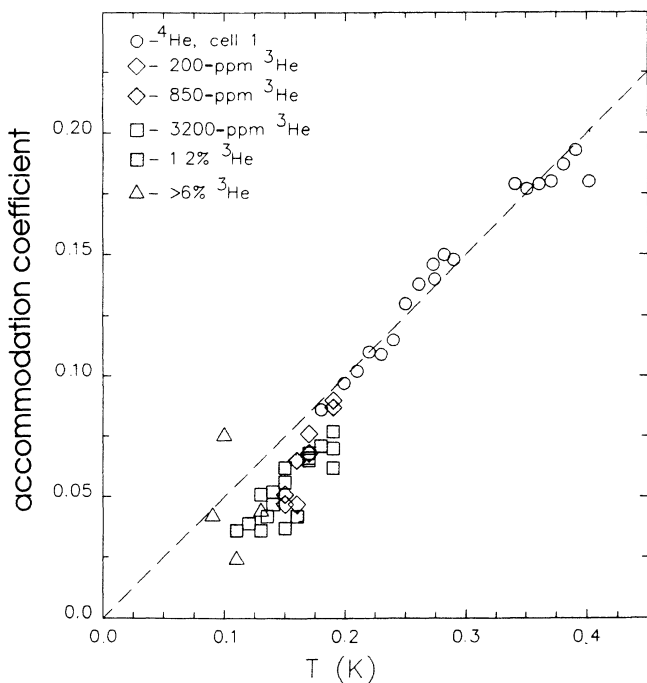


FIG. 4. Thermal accommodation coefficient vs temperature measured at different constant  $^3\text{He}$  concentrations: open circles, pure  $^4\text{He}$  surface from Ref. 1; open diamonds, 200 ppm of  $^3\text{He}$  in  $^4\text{He}$ ; solid diamonds, 850 ppm; open squares, 3200 ppm; solid squares, 1.2%; open triangles,  $> 6.4\%$ ; dashed line,  $\alpha=0.50T$ .

Interpretation of these results in terms of the conventional one-ripplon process seems attractive, but faces some difficulties. Ripplon damping in bulk  $^3\text{He}$  due to viscosity should suppress this mechanism. This may not

be a problem for the submonolayer films. For these samples, the lack of sensitivity to the presence of  $^3\text{He}$  may indicate that the long-range part of the surface potential dominates the sticking probability.

---

\*Present address: Department of Physics, University of California, San Diego, La Jolla, CA 92093.

<sup>1</sup>J. Helffrich, M. P. Maley, M. Krusius, and J. C. Wheatley, *Phys. Rev. B* **34**, 6550 (1986).

<sup>2</sup>B. W. Statt, *Phys. Rev. B* **32**, 7160 (1985).

<sup>3</sup>D. S. Zimmerman and A. J. Berlinsky, *Can. J. Phys.* **61**, 508 (1983).

<sup>4</sup>J. J. Berkhout, E. J. Wolters, R. van Roijen, and J. T. M. Walraven, *Phys. Rev. Lett.* **57**, 2387 (1986).

<sup>5</sup>V. Goldman, *Phys. Rev. Lett.* **56**, 612 (1986).

<sup>6</sup>Yu. Kagan, G. V. Shlyapnikov, and N. A. Glukhov, *Pis'ma Zh. Eksp. Teor. Fiz.* **40**, 287 (1984) [*JETP Lett.* **40**, 1072 (1984)].

<sup>7</sup>For a review on the properties of the free surface of liquid He, see D. O. Edwards and W. F. Saam, in *Progress in Low Temperature Physics*, edited by D. F. Brewer (North-Holland, Amsterdam, 1978), Vol. VIIA, p. 283.

<sup>8</sup>J. A. Yapple and R. A. Guyer, *Phys. Rev. B* **27**, 1629 (1983).

<sup>9</sup>R. Jochemsen, M. Morrow, A. J. Berlinsky, and W. N. Hardy, *Phys. Rev. Lett.* **47**, 852 (1981); M. Morrow and W. N. Hardy, *Can. J. Phys.* **61**, 956 (1983).

<sup>10</sup>D. O. Edwards, S. Y. Shen, J. R. Eckardt, P. P. Fatouros, and F. M. Gasparini, *Phys. Rev. B* **12**, 892 (1975).

<sup>11</sup>For a review on spin-polarized hydrogen ( $\text{H}_1$ ), see I. F. Silvera and J. T. M. Walraven, *Progress in Low Temperature Physics*, edited by D. F. Brewer (Elsevier, New York, 1986), Vol. X, p. 139.

<sup>12</sup>E. H. Kennard, *Kinetic Theory of Gases* (McGraw-Hill, New York, 1938), p. 315.

<sup>13</sup>J. Helffrich, M. P. Maley, M. Krusius, and J. C. Wheatley, *J. Low Temp. Phys.* **66**, 277 (1987).

<sup>14</sup>H. Doi, Y. Narahara, Y. Oda, and H. Nagano, in *Proceedings of the 17th International Conference on Low Temperature Physics, LT-17*, edited by U. Eckern *et al.* (North-Holland, Amsterdam, 1984), Part I, p. 405; Q. Li, C. H. Watson, R. G. Goodrich, D. G. Hasse, and H. Lukefahr, *Cryogenics* **26**, 467 (1986); M. S. Love and A. C. Anderson, *Rev. Sci. Instrum.* **58**, 1113 (1987).

<sup>15</sup>J. A. Helffrich, Ph.D. thesis, University of California at San Diego, 1987.

<sup>16</sup>D. Crum, D. O. Edwards, and R. E. Sarwinski, in *Proceedings of the 14th International Conference on Low Temperature Physics, LT-14*, edited by M. Krusius and M. Vuorio (North-Holland, Amsterdam, 1975), Vol. I, p. 423; I. B. Mantz, D. O. Edwards, and V. U. Nayak, *Phys. Rev. Lett.* **44**, 663 (1980).

<sup>17</sup>R. Radebaugh, in *Thermodynamic Properties of  $^3\text{He}/^4\text{He}$  Dilution Refrigerator*, Natl. Bur. Stand. (U.S.) Technical Note 362 (U.S. GPO Washington, D.C., 1967).

<sup>18</sup>H. M. Guo, D. O. Edwards, R. E. Sarwinski, and J. T. Tough, *Phys. Rev. Lett.* **27**, 1259 (1971).

<sup>19</sup>F. M. Ellis, J. S. Brooks, and R. B. Hallock, *J. Low Temp. Phys.* **56**, 69 (1984).